HAL open science

Numerical study of an experimental high-intensity prescribed fire across Corsican Genista salzmannii vegetation

Jacky Fayad, Lucile Rossi, Nicolas Frangieh, Carmen Awad, Gilbert Accary, François-Joseph Chatelon, Frédéric Morandini, Thierry Marcelli, Valérie Cancellieri, Dominique Cancellieri, et al.

To cite this version:

Jacky Fayad, Lucile Rossi, Nicolas Frangieh, Carmen Awad, Gilbert Accary, et al.. Numerical study of an experimental high-intensity prescribed fire across Corsican Genista salzmannii vegetation. Fire Safety Journal, 2022, 131, pp.103600. 10.1016/j.firesaf.2022.103600 . hal-04063905

HAL Id: hal-04063905

https://hal.science/hal-04063905

Submitted on 10 Apr 2023

HAL is a multi-disciplinary open access archive for the deposit and dissemination of scientific research documents, whether they are published or not. The documents may come from teaching and research institutions in France or abroad, or from public or private research centers.

L'archive ouverte pluridisciplinaire **HAL**, est destinée au dépôt et à la diffusion de documents scientifiques de niveau recherche, publiés ou non, émanant des établissements d'enseignement et de recherche français ou étrangers, des laboratoires publics ou privés.

Numerical study of an experimental high-intensity prescribed fire across Corsican Genista salzmannii vegetation

Jacky Fayad [a], Lucile Rossi [a], Nicolas Frangieh [a,*], Carmen Awad [a], Gilbert Accary [b], François-Joseph Chatelon [a], Frédéric Morandini [a], Thierry Marcelli [a], Valérie Cancellieri [a], Dominique Cancellieri [a], Dominique Morvan [c], Antoine Pieri [a], Gilles Planelles [e,f], René Costantini [e], Sofiane Meradji [d], Jean-Louis Rossi [a]

[a] *UMR CNRS SPE 6134, Université de Corse - CNRS, 20250, Corte, France*
[b] *Scientific Research Center in Engineering, Lebanese University, Museum Square, 1106, Beirut, Lebanon*
[c] *Aix-Marseille Univ, CNRS, Centrale Marseille, M2P2, Marseille, France*
[d] *IMATH Laboratory, EA 2134, Toulon University, 83160, Toulon, France*
[e] *SIS2B, Centre Administratif du Fango, 20200, Bastia, France*
[f] *Office National des Forêt – Corse - Unité Production Travaux - Responsable UP, France*

ARTICLE INFO

Keywords:
Winter wildfires
Field experiment
Fire behavior
Physical fire model

ABSTRACT

This paper reported a high intensity experimental fire conducted during a field-scale experiment on a steep sloped terrain (28°) as part of a winter prescribed burns campaign managed by the local firefighter service in the north-western region of Corsica. The rate of spread (ROS) of fire, measured using UAV cameras (thermal and visible), was evaluated at 0.45 m/s. The experiment was numerically reproduced using a completely physical 2D model, namely FireStar2D, and the comparison with the experimental measurements mainly concerned the fire ROS and the heat fluxes received by three distant targets placed at the end of the plot. The results analysis shows that the considered fire has a wind-driven regime of propagation with a fire intensity higher than 7 MW/m. The numerical results are in fairly good agreement with the experimental measurements, within 11% difference for the ROS and 5% for the heat fluxes, validating consequently the relevance of the numerical approach to tackle such high-intensity wildfires. Despite the unfavorable wind and humidity conditions for fire propagation (U = 1.67 m/s and RH = 82%), this experiment confirms that such fire can exhibit a dangerous behavior due to the steep slope of the terrain.

1. Introduction

Wildfires represent the main cause of natural capital damage in Mediterranean regions and one of the main drivers of landscape. There are five regions over the world that present a Mediterranean climate: the Mediterranean basin, California, Chile, South Africa and Australia (the South and South-West). These zones occupy almost 2% of Earth surface. The Mediterranean climate is characterized by a high seasonality that can be summarized as hot, dry summers, and mild wet winters [1]. Changes in climatic and weather conditions are one of the major reasons for the increase in wildfire risk [2,3]. In recent decades, Mediterranean regions tend to be warmer and drier [4], and has experienced frequent heat waves [5]. Moreover, studies have shown that the region around the Mediterranean Sea has been identified as one of the most vulnerable regions around the world to climate change [6]. So, Mediterranean climate conditions are prone to fire ignition and propagation in a very flammable vegetation [7,8] with a longer wildfire season. It is generally recognized that these conditions constitute one of the major sources of increasing forest fires risk [9,10] and burned area [11]. In the next century, global temperatures are expected to be warmer than current levels and severe droughts more frequent [12]. Thus, the Mediterranean regions will potentially be more affected by wildfire risk [9]. The last years witnessed many high-intensity forest fire incidents caused mainly by the heat wave and the extreme drought conditions [10]. For instance, the catastrophic fires of 2018 summer in Greece [13], fanned by strong wind and high temperature, grew rapidly destroying houses and reaching the sea and it posed a risk to the safety of a large oil refinery. The severe fires of Portugal (2007), southern Italy (2005), and Greece (2003) are further examples high intensity forest fire incidents. Other

* Corresponding author.
E-mail address: frangieh_n@univ-corse.fr (N. Frangieh).

Nomenclature

C_p	Vegetative fuel specific heat (J/kg. K)
C_{p0}	Ambient air specific heat (J/kg. K)
D	Fuel particle diameter (m)
e	Fuel bed depth (m)
g	Earth acceleration (m/s^2)
I	Radiation intensity (W/m^2)
I_B	Byram fireline intensity (W/m)
I_{BExp}	Byram fireline intensity evaluated experimentally (W/m)
I_{BNUM}	Byram fireline intensity evaluated numerically (W/m)
FMC	Fuel moisture content (mass of water/mass of dry fuel)
Nc	Byram number
ROS	Rate of spread (m/s)
RH	Relative humidity
s	Surface area to volume ratio (m^{-1})
s_g	Absorption coefficient of gas/soot mixture
T_0	Ambient temperature (K)
T	Gas mixture temperature (K)
T_a	Target temperature (K)
T_s	Solid particle temperature (K)
U	Experimental wind speed (m/s)
U_x	Wind speed at x meters above the ground (m/s)
ΔH_c	Fuel yield heat (J/kg)
ΔH_t	Fuel pyrolysis heat (J/kg)
$\dot{w}_{pyr}$	Rate of dry material pyrolysis (kg/m.s)
$\dot{w}_{char}$	Rate of charcoal combustion (kg/m.s)
w_a	Weight of fuel consumed in the active flaming front (kg/m^2)
$\dot{m}$	Vegetation degradation rate (kg/m.s)
h_{conv}	Convective heat transfer coefficient (W/m^2.K)
B	Stephan-Boltzmann constant (W/m^2.K^4)
J	Total irradiance (W/m^2)
Pr	Prandtl number of gas mixture
Re	Reynold number of fuel particles
Lc	Characteristic length (m)
Qc, Qr	Convection and radiation heat transfer rates between the flame and the vegetation (W/m)
$Qconv$, $Qrad$	Convective and radiative heat fluxes received by the target (W/m^2)
ρ_0	Ambient air density (kg/m^3)
ρ_v	Fuel particle density (kg/m^3)
β	Volume fraction of the solid phase
β_g	Volume fraction of the gaseous phase
σ	Solid fuel load (kg/m^2)
ϵ	Thermal emissivity
λ	Thermal conductivity of gas mixture (W/m.K)

extreme fires could blaze during winter, caused by the early melting of winter snows and the late rains in the fall season. The cold-weather wildfires are becoming more common during the last years, such as the recent winter wildfire in Colorado that occurred in December (2021). In general, extreme fires are very dangerous since their behavior is unpredictable and uncontrollable [14]. This type of fires can be characterized by a high rate of spread (ROS), by spotting fires, or by a sudden change of fire behavior [15] as well as by a high fireline intensity that could exceeds the 10 MW/m, the threshold beyond which a fire becomes erratic and uncontrollable [16]. Therefore such fires constitute a threat for the population, assets, and natural values, resulting in important negative socio-economic and environmental impacts [12,16]. Hence, Mediterranean region is in a new wildfire context because fire risk is likely to increase substantially in the future, and extreme catastrophic wildfire events could occur more frequently. The real problem here is that these extreme wildfire events tend to overwhelm suppression efforts. Thus, this new context requires adapted policies to shift the focus from suppression to prevention, as called by the Sendai Framework for Disaster Risk Reduction 2015–2030 [17].

Wildland fire suppression and prevention requires a good knowledge of the physical mechanisms governing fire behavior (ignition, initial development, spread). Therefore, local measurements of fire dynamics in field-scale experiments of wildland fires are highly useful. This is true either for understanding the mechanisms driving fire spread that result in the observed macroscopic behaviors or in terms of providing comparison points for numerical tools, such as detailed physics-based fire models. Wide variety of experimental and numerical studies on wildfire behaviour exists in the literature. For instance, Finney et al. [18] performed wind tunnel laboratory fires spreading through laser-cut cardboard while Frangieh et al. [19] investigated these fires later on using a CFD Physical model; Liu et al. [20] studied the effect of slope on spread of a linear flame front over a pine needle, experimentally and numerically, at laboratory scales; Awad et al. [21,22] studied numerically and experimentally at small scale the moisture content threshold of extinction; Viegas et al. [23] investigated experimentally junction fire, at laboratory and small field cases, where these results were compared also to a previous wildfire and later on simulate the evolution of this kind of fires where reproduced numerically using CFD based numerical models [24]; Marsden-Smedley et al. [25] performed a burning program, based on experimental and prescribed fires in order to develop fire behaviour prediction models; Xavier et al. [26] investigated the temperature and the heat fluxes of experimental field fires spreading through small flat parcels; Bulter et al. [27] reports the fire intensity rate of spreads of low-intensity fires spreading in longleaf pine. The idea of citing these studies, is to point that most of the experimental studies were carried out for laboratory scale and/or small terrain (flat or with moderate slope) and under moderate wind speed resulting consequently in a low ROS and low fire intensity; not to mention that most of them focus on specific aspects of fire behavior. This could be justified as follows: on the one hand, despite the considerable progress that has been made in the characterization of wildland fire spreading [37–39], experimental field-scale fires remain extremely problematic in terms of security and fraught with numerous difficulties. Such fires are often subject to the vagaries of the weather and variations in the vegetation and land topography [40]. The interaction of these, and even with the fire itself, can result in seemingly capricious behavior. On the other hand, attempting to obtain direct measurements of the characteristics of such fires with pre-positioned instrumentation is similarly beset by practical problems, including being in the right location at the right time, safely, to make useful observations and measurements of critical quantities during the fire propagation. Consequently, obtaining repeatable conditions in the field is challenging, often requiring a large number of replicate experiments to reduce statistical error, which is costly and difficult to achieve. Therefore, relevant experimental data on high-intensity wildfires is of paramount interest and experiments at the field-scale are highly valuable.

In this context, the main objective of this study is to present experimental data of a fire carried out at large scale field, having an important slope, resulting in a high fire intensity. This field-scale experiment has been conducted at the north-western region of Corsica during a prescribed fire campaign in March 2021, where prescribed burnings are commonly used in Corsica [26]. In order to understand and investigate the different phenomena encountered in this type of fires, the experimental results are compared to the prediction provided by a complete physical model, namely FireStar2D [28]. FireStar2D is employed to assess the fire front dynamics, in particular to accurately evaluate the

fire intensity, which is always a challenge for field-scale experiments. In addition, the rate of spread and the heat fluxes received by three distant targets placed at the end of the plot are also examined and compared to the experimental data. Consequently, these data could contribute to a better understanding of these fires and serve to validate numerical models for this fire category.

In the next section the experimental method is thoroughly described, followed by the modeling approach that was used. Then, the experimental results are detailed as well as numerical results in two separate sections. Finally, an analysis and a discussion of the relevance and the significance of these results are presented.

2. Experimental method

2.1. Site description

In order to obtain field-scale data, a fire spread experiment was carried out as a part of a winter campaign of prescribed fires conducted at the north-west coast of Corsica (France), in March 2021. The experimental site is located 10 km from the sea, in an uneven terrain (42°32′38″N, 8°58′07″E) at 990 m above sea level and facing east-northeast (Fig. 1a), and it was selected based on two criteria. First, the plot has a steep slope in order to generate high intensity fire close to wildfire conditions; the average slope of the terrain is 28 ± 2°. This value was obtained by precisely measuring the coordinates of five points positioned 25 m apart along the centerline of the plot, namely poles 1, 2, 3, 4 and thermocouple 1, as shown in Fig. 1b. The coordinates of these points were determined using a high-precision Global Navigation Satellite System (GNSS). Second, the plot has a roughly homogeneous vegetation with high vegetation cover (coverage >90%). The vegetation was mainly composed of 0.6 m high mountain shrubs (*Genista salzmannii*) with few fuel discontinuities. The vegetation plot to be burned was in the shape of a rectangle, about 30 m wide and 130 m long along the main slope direction.

2.2. General overview of the experimental protocol

The limits and orientation of the vegetation plot (30 m × 130 m) were chosen according to the main slope direction to favor a high intensity fire. The experimental protocol was developed to investigate the main thermal properties and behavior of a fire. Thus, pre-fire vegetation samplings were done to measure the FMC, and measuring devices have been deployed in the field (Fig. 2). Six heat flux sensors and four thermocouples were placed in the vegetation free area to record the radiant/total heat fluxes and air temperature, respectively. Two video cameras were located on the sides to investigate the flame geometric characteristics. The fire front propagation was also recorded from above using a drone-mounted Visible-IR camera. The wind properties and ambient conditions were also recorded using a portable weather station. A linear ignition was performed at the bottom of the plot resulting in an upslope fire spreading.

2.3. Characterization of the vegetation and meteorology

As mentioned previously, this site was selected for the apparent structural homogeneity of its vegetation, mostly composed of Genista salzmanniin, whose thermo-chemical properties (such as specific, yield, and pyrolysis heats) can be found in literature [29]. On the other hand,

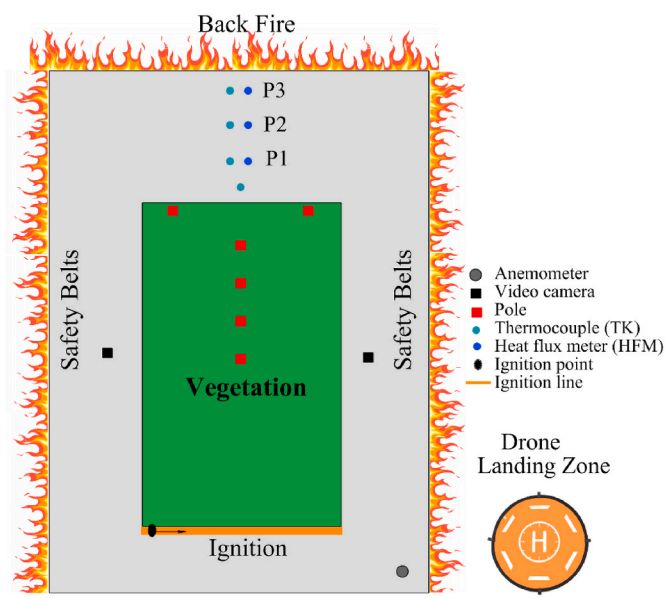

Fig. 2. Schematic view of the experimental plot and the location of the measuring devices.

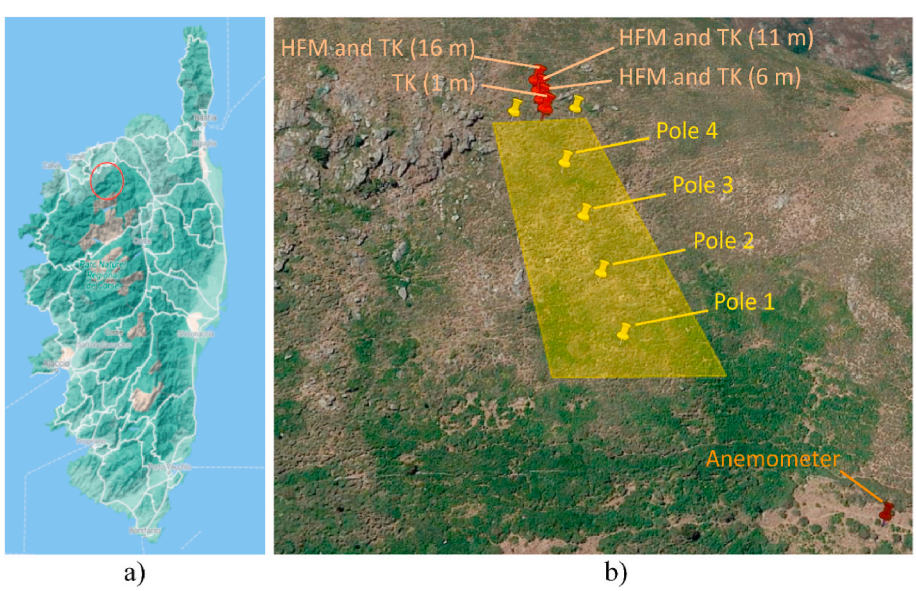

Fig. 1. Experimental fire site in Corsica island: (a) location on the map; (b) view by Google earth and main GNSS measurement points.

other physical properties, such as the FMC, the packing ratio, the fuel height, and the fuel-load density are specific to the geographic area and depend on weather conditions. Fuel height was evaluated by averaging 20 different measurements of the distance between the ground and the average top of the vegetation. Fuel characterization was carried out by fuel sampling and applying a destructive inventory using a cube methodology [30]. Before ignition, samples of dead and live fuel elements with diameters less than 6 mm (assumed to mainly contribute to fire spread) were collected in double-seal plastic bags. For the FMC determination, the collected samples were considered as consisting of a single fuel type, thus the reported FMC corresponds to an average value covering both the dead and the living fuels. The FMC was calculated based on a dry weight basis taking into account condensation onto the bags. Fuel samples were oven dried at 60 °C for 48 h for moisture content determination [21]. Oven-dry weight of the collected material was determined after laboratorial processing and expressed in terms of fuel loading. The volume fraction (packing ratio) was then obtained by dividing the fuel load by the product of the average vegetation height and the particle density.

The Ambient weather conditions were recorded less than 50 m from the centerline of the plot (Fig. 1b). The wind velocity and direction were obtained using a two-dimensional ultrasonic anemometer (WS425, Vaisala) at 3 m above the ground to reflect the average wind acting on the fire front. The anemometer was located downhill of the vegetation plot to minimize the influence of the fire on the wind measurements. Wind data were recorded using a data logger (CR3000, Campbell Scientific) at a sampling rate of 1 Hz. Air temperature and relative humidity were monitored during fire spread using a weather meter (Kestrel 5500, Kestrel Instruments).

2.4. ROS evaluation: drones and vision technology

Given the plot width and field constraints, the ignition was conducted, slowly and unsymmetrically, starting from the left side to right side of the plot. During the experiment, the fire front propagation was recorded from above using a drone and from the side using two cameras (GoPro Hero4, GoPro Hero+) located on the ground. The drone used was DJI M210 with a Zenmuse XT2 camera featuring both a FLIR longwave infrared (7.35–13.5 μm spectral band) camera and a visual camera, with resolutions of 3840 × 2160 and 640 × 512 pixels respectively. The drone was located at a height of about 100 m, which allowed top shots of the fire spread across the whole vegetation plot. In order to simplify the video tracing of the fire front location, four poles were placed, before ignition, on four equidistant reference points (~25 m apart) as shown in Fig. 1b. These points were also used to evaluate the plot slope. The ROS was then determined by recording the times at which the fire front had crossed each reference pole; this allowed the evaluation of the ROS when the fire had reached a steady state propagation.

2.5. Heat flux measurement

The total and radiant heat fluxes emitted from the flame front during the fire spread were measured with 3 pairs of Medtherm transducers (16H and 64 Series, Medtherm Corp, Huntsville, AL, USA) located uphill on the vegetation free area. A sapphire window was added to the radiant heat flux transducer to eliminate the convective heat being transferred to the sensing area. These transducers were calibrated by the manufacturer in the range 0–200 kW/m^2 and had a response time less than 0.25 s. Thus, experimental studies have shown that a maximum total heat flux of 112 kW/m^2 could be reached ahead of the fire front [26]. The radiant and total heat flux transducers had a view angle of 150° and 180°, respectively. They were oriented towards the fire and in the slope direction (Fig. 3). The pairs of heat flux transducers were fixed on 0.5 m high supporting rods located at 6, 11, and 16 m from the upper limit of the vegetation plot. Air temperature was also recorded using K-type thermocouples with a 2.5 μm-diameter grounded junction. Four thermocouples were also fixed on supporting rods located at 1, 6, 11, and 16 m from the upper limit of the vegetation plot (Fig. 2). The heat flux gauges and thermocouples were plugged into a power-supplied data logger (CR3000, Campbell Scientific) buried 0.3 m into the ground to protect it from the fire. Extension cables of the sensors were insulated by Teflon coating and aluminum foils (Fig. 3). They were buried into the ground up to the data logger. The analogue signals from all transducers were recorded at a sampling rate of 1 Hz.

Fig. 3. Radiant and total heat flux sensors and thermocouple fixed on supporting rod and protected by aluminum foils.

3. Modeling and numerical method

In order to test the relevance of numerical simulation in the case of high-intensity wildfires, a simulation was carried out using a completely physical 2D model, namely FireStar2D. Indeed, having an important fire-front width in this present case allows good predictions using FireStar2D model that assumes an infinite ignition line. In addition, this 2D model was validated from calculations carried out at different scales for homogeneous fuel beds and was compared to experimental results as well as to empirical and semi-empirical models [21,28,31]. FireStar2D model appears to be suitable for operational works since it provides valuable results and requires much less simulation time compared to the 3D model version.

The mathematical model used in FireStar2D is based on a multiphase formulation [32], it consists in a first step in space-averaging the conservation equations (energy, mass, momentum …) governing the behavior of the coupled system formed by the vegetation and the surrounding atmosphere. This averaging is performed on elementary control volumes including both the gaseous phase and the solid phase (the vegetation). Thus, the model consists of two parts that are solved on two distinct grids. The first part consists of the equations governing the reacting and turbulent flow of the gas mixture of fresh air and the gaseous products resulting from the degradation of the solid fuel (by drying, pyrolysis, and heterogeneous combustion) and the homogeneous combustion in the flaming zone. The second part consists of the equations governing the state and the composition of the solid phase subjected to an intense heat flux coming from the flaming zone. Therefore, the rate of fire spread, and more generally, all variables characterizing fire behavior (flame geometry, fire intensity, etc.) are obtained from the resolution of the balance equations governing the various interactions occurring between the vegetation, the surrounding atmosphere, and the

flame [32,33]. The details of FireStar2D model have been thoroughly described in previous publications, and the reader is invited to consult references [22,28,34–36] for more information about this 2D model and for a comparison with other wildfire tools available within the community.

The 2D computational domain used for the simulations was 200 m long and 35 m high (Fig. 4), and the homogeneous vegetation layer, of height $e = 0.6$ m and 100 m long was located 20 m from the domain inlet. The main physical characteristics of the vegetation layer are given in Table 1. The solid fuel particles were assumed to behave as a black body and a vegetation family of cylindrical shape was considered. The shape of the fuel particles is used for the description of their regression law and for the estimation of the heat transfer coefficients. Both the solid-phase and the fluid-phase grids were characterized by cells sizes below the radiation extinction length scale [31,37] the vegetation given by $4/s\beta$, where s is the surface to volume ratio of the vegetation (m^{-1}) and β is the volume fraction of the solid phase (see Table 1); this characteristic length is equal to 0.42 m in present case. This value should not be exceeded in order to avoid fire extinction especially in the case of radiation-dominated fire propagation (i.e., when the wind speed is low to moderate). Ignition was obtained by the injection of carbon monoxide at 1600 K from the ground (between 20 m and 22 m) during 5 s and with a constant velocity of 1 m/s [19,22,38,39]. Ignition was activated after reaching a statistically-steady profile of the turbulent boundary-layer inside and above the fuel bed [31] which required 30 s of simulation time.

The simulation was carried out for a 10 m open wind speed $U_{10} = 1.98$ m/s (which corresponds to 1.67 m/s at 3 m above ground by assuming a one-seventh power wind velocity profile) and for a slope angle $\alpha = 28°$. The domain inclination angle was specified through two non-zero components of gravitational acceleration: $g_x = -g\sin(\alpha)$ and $g_z = -g\cos(\alpha)$, where $g = 9.81$ m/s^2 is Earth gravity.

The ROS represents one of the main parameters that characterize wildland fire behavior. Using FireStar2D, the ROS is obtained from the slope of the curve of the pyrolysis front position (during the time), at the fuel-bed surface, once fire propagation had become steady. One other feature of FireStar2D, is the possibility to evaluate any characteristic of the fire at any time and any position in the computational domain. On the one hand, this model allows the evaluation of the convection and radiation heat transfer rates between the flame and the vegetation (W/m of fuel-bed width) [28], thus to identify the dominant heat transfer mode between the flames and the vegetation layer as well as its effect on fire behavior. On the other hand, this model allows the evaluation heat fluxes (radiative and convective) received by a target (W/m^2) at a given position, particularly to assess the heat fluxes recorded by the three flux meters located at the end of the plot. To evaluate the convection heat flux received by the flux meter a Newton's law of cooling [40], given by Eq. (1), was employed. In this equation, $(T_0 - T_a)$ represents the difference between the gas mixture temperature and the target temperature (assumed to be the ambient temperature) and h_{conv} is the convective heat transfer coefficient.

$$Q_{conv} = h_{conv}(T_0 - T_a) \tag{1}$$

h_{conv} was calculated from the correlation given by Eq. (2) for forced convection over the fluxmeter gauge foil assumed to behave as a flat plate, where the flow can be considered as laminar at the gauge surface even if the flame is strongly turbulent [26]; L_c (m) is the characteristic length that depends on the target shape (equal to the fluxmeter gauge diameter in this case), k is the thermal conductivity (W/m.K) of the gas mixture, Re is the Reynolds number based on L_c, and Pr is the Prandtl number of the gas mixture.

Table 1
Main average properties of Genista salzmannii.

Particle density, ρ_v (kg/m^3)	970
Volume fraction, β	0.00309
Fuel moisture content, FMC (%)	65
Fuel bed depth, e (m)	0.6
Fuel load, σ (kg/m^2)	1.8
Thermal capacity, Cp (J/kg/K)	1648
Yield heat, ΔH_c (J/kg)	1.8620×10^7
Pyrolysis heat, ΔH_t (J/kg)	1.3917×10^7
Surface-area to volume ratio, s (m^{-1})	3100
Thermal emissivity, ϵ	1
Vegetation family shape	Cylindrical

$$h_{conv} = \frac{k}{L_c} 0.664 \ \mathrm{Re}^{1/2} \ \mathrm{Pr}^{1/3} \tag{2}$$

The Fireline intensity cannot be experimentally measured, but only estimated through other measured quantities. The experimental fireline intensity can be evaluated from Eq. (3) (Byram's intensity [41]), where w_a is the weight of fuel consumed in the active flaming front (kg/m^2), and ΔH_c is the heat yield of the fuel (estimated at about 18,620 kJ/kg, see Table 1). In operational conditions, the consumed fuel w_a , is evaluated from the fuel load (σ) weighted by a combustion efficiency, i.e., $w_a = \mu\,\sigma$, where μ is the percentage of the fuel weight actually consumed in the active flaming front and effectively contributed to fire propagation.

$$I_{BExp} = \Delta H_c . w_a . ROS \tag{3}$$

This experimental method is often inaccurate, because it is based on visual estimation of the burned vegetation during the fire [42]. These difficulties do not exist in the numerical evaluation of the fire intensity from the Heat Release Rate (HRR) given by Eq. (4) [31], where $\dot{m}$ (kg/m.s) is the vegetation degradation rate evaluated by the summation of mass losses due to pyrolysis and charcoal combustion where ΔH_c is the vegetation heat yield (J/kg).

$$I_{BNum} = \dot{m} . \Delta H_c \tag{4}$$

The vegetation degradation rate is evaluated in FireStar2D [31] from Eq. (3), where $\dot{w}_{pyr}$ and $\dot{w}_{char}$ represent the rate of dry material pyrolysis and charcoal combustion.

$$\dot{m} = \dot{w}_{pyr} + \dot{w}_{char} \tag{5}$$

Using the fire line intensity calculated from the equation above, it is then possible to evaluate the Byram's convective number defined as the ratio between the buoyancy force and the wind inertial force [43]. Byram's convective number is often used as an indicator of the fire propagation regime. Large values of Byram's number ($N_c > 10$) are normally obtained in fires governed by thermal plumes (plume-dominated fires), where heat transfer between the flame and the unburned

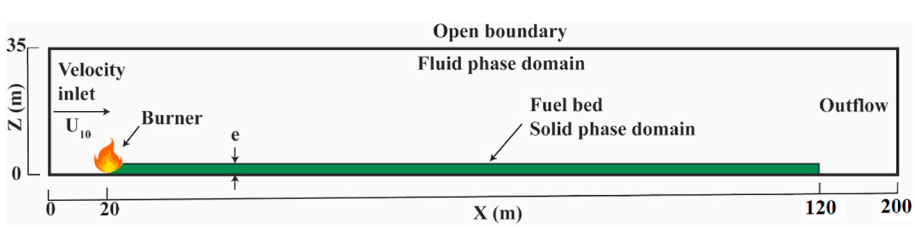

Fig. 4. Computational domain and boundary conditions used in the 2D simulation of the experimental fire.

vegetation is dominated by radiation. Whereas small values of Byram's number ($N_c < 2$) are obtained in fires piloted by inertial effects (wind-driven fire), with a more important contribution of convection heat transfer [44]. Byram's number is given by Eq. (6), where I_B is the fire intensity, g is the gravity acceleration, $\rho_0 = 1.26$ kg/m^3 and $C_{P0} = 1004$ J/kg.K are air density and specific heat at the ambient temperature $T_0 = 279$ K, and U_{10} is the 10 m-open wind velocity.

$$N_c = \frac{2g\, I_B}{\rho_0 C_{P0} T_0 (U_{10} - ROS)^3} \tag{6}$$

For a fire propagating uphill, an effective wind speed acting in the direction of fire propagation should be considered to include the effect of the slope on the fire regime [45]; this effective wind speed is given by Eq. (6), where w_c represents the buoyant flame velocity [43] given by Eq. (8).

$$U_e = U_{10} + w_c \ \sin\alpha \tag{7}$$

$$w_c = \left(\frac{2g\, I_B}{\rho_0 C_{P0} T_0}\right)^{1/3} \tag{8}$$

4. Experimental results

4.1. Fuel characteristics and wind conditions

A single type of vegetation particle was considered in this study [29]. The vegetation characterization, described in section 2.1, resulted in FMC, e, and σ equal to 65%, 0.6 m, and 1.8 kg/m^2 respectively (Table 1).

The fire experiment occurred between 12:49 and 13:04. During this period, the average wind speed was 1.67 ± 0.54 m/s. It should be noticed that the average wind direction (60 ± 14°) was aligned with the main slope direction and it exhibited few fluctuations. The average air temperature and relative humidity were 6 °C and 82%, respectively.

4.2. Rate of spread

Fig. 5 shows the fire front position at different instants during the fire propagation, and Table 2 reports the time lapses taken by the fire to cross consecutive poles. For the first 22 s, just after the establishment of the ignition line, estimated at t = 12:53:30, the fire propagated with ROS equal to 1.136 m/s and then it slowed down to 0.423 m/s before reaching a quasi-steady propagation speed between the last three poles (Pole 2 – Pole 4) with a ROS equal to 0.45 m/s.

Table 2
Time lapses of fire propagation between consecutive poles.

	Distance separating poles (m)	Time lapse (s)	ROS (m/s)
Ignition line - Pole 1	25	22	1.136
Pole 1 - Pole 2	25	59	0.423
Pole 2 - Pole 4	50	111	0.45

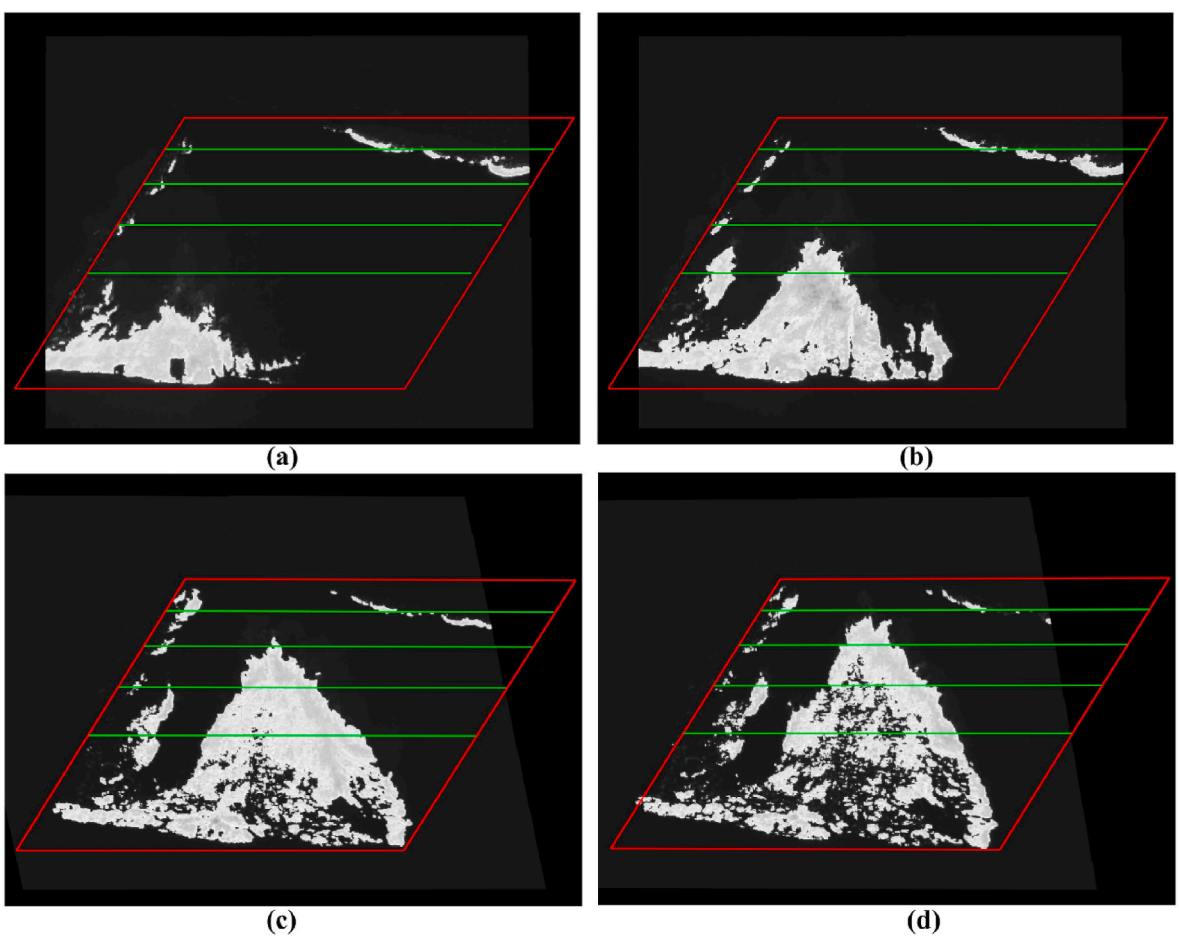

Fig. 5. Infrared images of the fire front travel between equidistant positions (the green lines passing through prefixed poles) at different times taking t = 0 s at 12:49 (fire start time): (a) t = 140 s; (b) t = 242 s; (c) t = 360 s; (d) t = 422 s. (For interpretation of the references to colour in this figure legend, the reader is referred to the Web version of this article.)

4.3. Heat fluxes and fireline intensity

Fig. 6 shows the time evolution of the radiative and total heat fluxes received by the different flux meters. Before t = 3700s, the time when fire front reached the end of the plot, flux meters were not sensitive to the heat produced by the fire. These heat fluxes outputs are later on investigated in the numerical results section.

According to Eq. (3), if all the vegetation was supposed to be consumed during the fire propagation, then $\mu = 1$ and $w_a = \sigma = 1.8$ kg/m^2 (see Table 1), consequently $I_{BExp} = 15.082$ MW/m. By visually comparing the plot vegetation before and after burning (see Fig. 7) the percentage of fuel weight consumed was estimated to $\mu \approx 70$ %; this results in $I_{BExp} = 10.5$ MW/m from Eq. (3).

5. Numerical results

5.1. Rate of spread and heat fluxes

FireStar2D predicts a ROS of about 0.5 m/s (Fig. 8), which is in agreement within 11% difference with the experimental value.

To identify the dominant heat transfer mode between the flames and the vegetation, the time evolution of the total rate of heat transfer (by radiation and convection) between the flame and the vegetation, integrated across the whole domain, is reported in Fig. 9.

On the other hand, the radiant and the convective heat fluxes received by three vertical targets located at 6 m, 11 m, and 16 m from the end of the vegetation plot are shown in Fig. 10 (respectively P1, P2 and P3). Fig. 11 presents the radiative heat fluxes obtained numerically at different sensor's positions, along with the experimental measurements, when the fire front reaches the end of the vegetation plot. Fig. 12 reports the radiative heat flux, obtained in Fig. 11, for the three sensors at t = 183.7 s. This figure, presented at logarithmic scale, shows a quasi-linear diminution of the radiative heat flux with respect to the target positions. The time-averaged ratio of the radiative heat flux to the total heat flux (i.e., convective and radiative), evaluated for the three flux meters (see Table 3), show a good agreement between experimental and numerical values within 5% difference.

5.2. Fireline intensity and fire regime

The experimental evaluation of I_B is rough because of the uncertain estimation of the total fuel load consumed by the fire in Eq. (3). The evaluation of the fireline intensity, according to Eq. (4) and Eq. (5), once fire propagation had become steady results in $I_{BNum} = 7.665$ MW/m.

Using the measured U_{10} value to evaluate Byram's convective number, Eq. (6) results in $N_c = 114$, which indicates a plume-dominated regime. Whereas using the value of U_e instead of U_{10} in Eq. (6) gives a $N_c = 3.24$, shifting substantially Byram's convective number toward the wind-driven fire range. The fire regime is further illustrated by Fig. 13 showing cuts of the temperature and the flow fields (streamline) in the vertical plane where the flow affects significantly the rise of the flame plumes by pushing the hot gases toward the unburned vegetation.

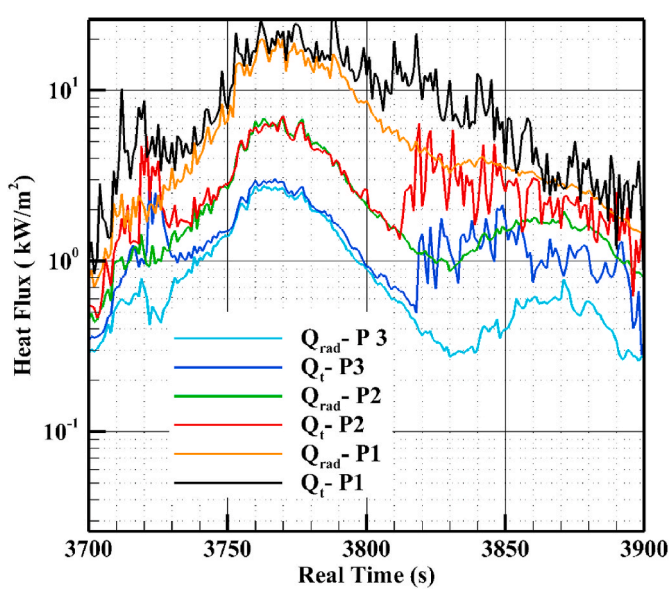

Fig. 6. Time evolution of the radiative and total heat fluxes obtained experimentally at the different target positions.

6. Discussion

6.1. Rate of spread

The transitory phase of the experimental ROS, before its establishment, could be due: first to an excess of gasoline poured to ignite the fire line (using drip torches) and second to the unsymmetrical ignition process (for safety considerations) applied in this prescribed fire. Because of this unsymmetrical ignition, fire starts moving at the departure ignition side (left side of the plot) with a higher speed than the rest of the fireline ignited progressively, but due to low wind speed conditions, the fire front was then established along the plot perimeter (see Fig. 5) to propagate after that with a quasi-steady speed of 0.45 m/s.

Concerning the 11% relative error between the experimental and the numerical values of the ROS, two factors can explain this difference: (1) in the numeric simulation, a homogeneous vegetation layer was considered, which is not the case in the experiment; (2) in 2D simulations, the fire front constitutes a uniform thermal barrier, while the fire front is in reality structured as a succession of peaks and troughs, allowing for the air flow to find a way across it [19,46]. Nevertheless, an 11% error is often considered acceptable for fire spread models [47].

6.2. Heat fluxes

The experimental radiative and total heat fluxes, reported in Fig. 6, are almost equal at the early stages (for the first 100 s) for all three targets. Then, the difference between the total heat flux (Q_{tot}) and the radiant one (Q_{rad}) becomes more pronounced, which is due to the existence of convective heating mechanism ahead of the fire front.

Fig. 9 shows that the convection is the main mechanism of heat transfer in this case. This is mainly due to the steep slope and the resulting thermal plume trajectory with respect to the fuel bed. Preheating of the unburned fuel mainly by convection (i.e., by direct contact with the hot gases) accelerated the fire front and led to a relatively high ROS despite the unfavorable propagation conditions. Nevertheless, even if the radiation is not the dominant heat transfer mode, it remains an important mechanism and contributes to 30% of the total rate of heat transfer received by the vegetation located ahead of the flame as shown by Fig. 9 and reported in the literature [48].

Both the numerical and the experimental radiative heat flux reported in Fig. 10 show the same levels of the radiative flux at the different target points. The discrepancy between the experimental data and numerical evaluation of the radiative heat flux is more pronounced at position P1 (the closest to the fire front) and is mainly due to the direct contact with the flame, whereas the differences are much less pronounced at positions P2 and P3.

Table 3 shows that the contribution of the radiative heat flux received by distant targets is dominant and exceeds 93% for the two furthermost points (P2 and P3). Despite the same order of magnitude, the radiation contribution at position P2 exceeds that at position P3. This slight difference could be due to the coherent turbulence structures present near the last target (see Fig. 10) which makes it in contact with the hot gases more than P2 target. Consequently, this increases the convective heat transfer, making the radiative contribution more

Fig. 7. Plot vegetation: (a) before burning and (b) after burning, allowing a visual estimation of the percentage of fuel consumed by the fire.

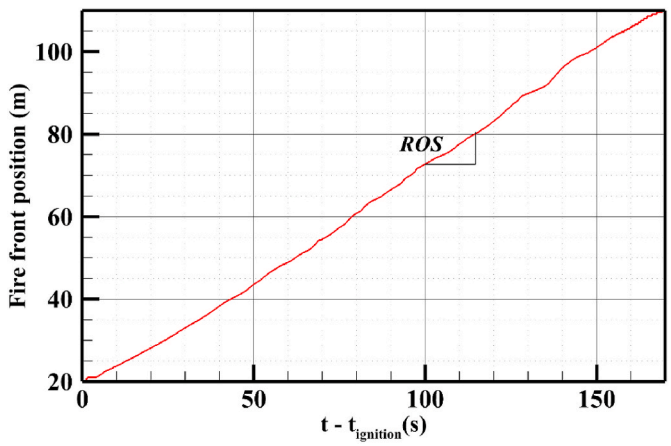

Fig. 8. Position versus time of the furthermost point of the pyrolysis front at the fuel-bed surface obtained by FireStar2D after ignition at t = 30 s.

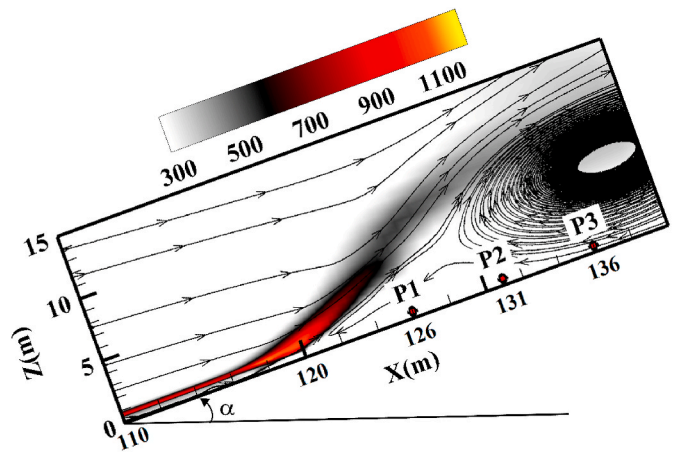

Fig. 10. Temperature field and streamlines obtained numerically as the fire approaches of the three targets positions points located ahead of the fire front.

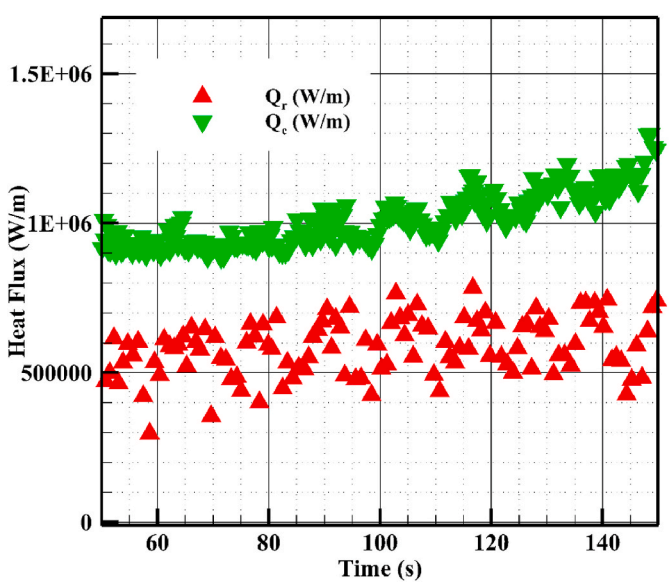

Fig. 9. Time evolution of the convection and radiation heat transfer rates between the flame and the vegetation evaluated with FireStar2D.

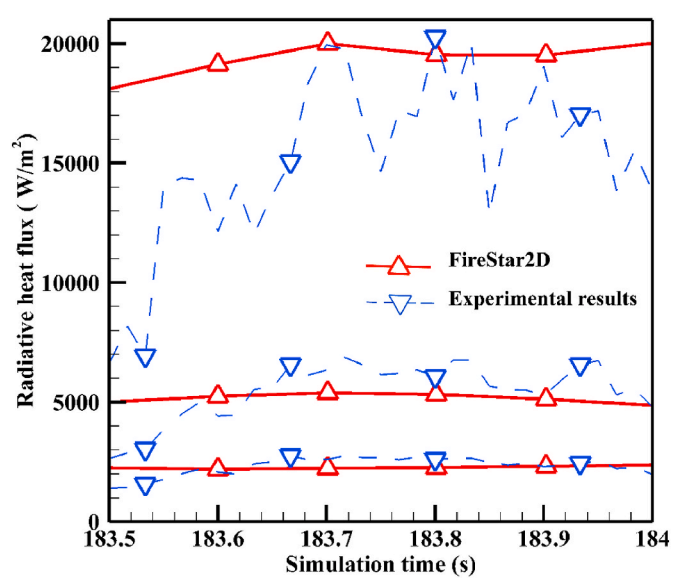

Fig. 11. Numerical and experimental values of the radiative heat flux at the different target positions when the fire front reaches the end of the plot.

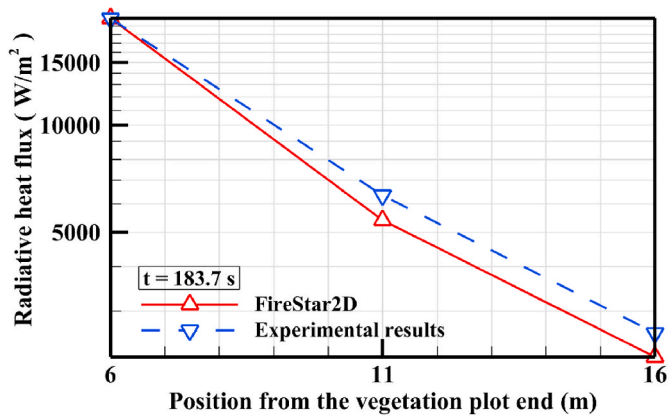

Fig. 12. Numerical and experimental radiative heat fluxes at different targets positions ahead of the fire front (P1 = 6 m, P2 = 11 m and P3 = 16 m), at t = 183.7 s.

Table 3
Time-averaged ratio of the radiative heat flux to the total one evaluated experimentally and with FireStar2D at the different target positions.

Position	Q_{rad}/Q_{tot} *FireStar2D*	Q_{rad}/Q_{tot} *Experiment*
1	0.796	0.845
2	0.993	0.971
3	0.961	0.930

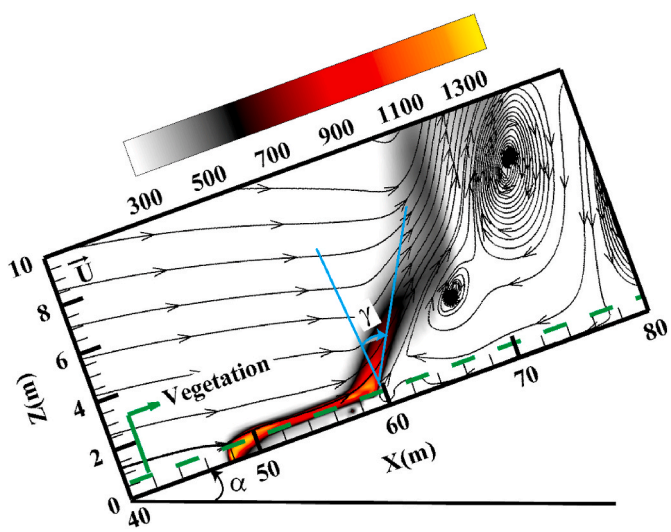

Fig. 13. Temperature field and flow streamlines obtained numerically in x-z plane.

important at position P2 than P3.

6.3. *Fireline intensity and fire regime*

Fireline intensity is usually used as an index to characterize the fire intensity rating (or fire severity or the suppression difficulty), such as in Ref. [48] where the classification was obtained for eucalypt forests. Whatever the evaluation method of the fire intensity (I_{BNum} = 7.665 MW/m and I_{BExp} > 10.5 MW/m assuming a percentage of fuel consumption greater than 70%), the considered fire falls into the category of "very high" fire severity, according to Ref. [48] with a wind driven regime of propagation. It is worth mentioning here that the evaluation of Byram's convection number using of the effective wind U_e instead of U_{10} in Eq. (6) was required to account for fire propagation on sloped terrain. Thus, in this specific case and due to the steep slope, the flame attachment to the ground results in a wind-driven-like regime of fire propagation [31,44].

However, for this fire class, all available fuel is usually consumed, which was not the case for this fire. Fire severity and its effect on soil also depends on fire residence time [15,49] which is also related to the ROS. Due to the relatively large value of the ROS obtained in this case (0.45 m/s), only partial combustion was achieved and less fuel was burned in the flaming front compared to a slower-moving fire where more fuel is consumed in the flaming front [50]. Also, the amount of consumed fuel is affected by the FMC (especially when it exceeds 40%), where the time required for the fire to consume the solid fuel increases with the FMC [51]. However, due to the important slope, fire moves relatively fast, and its residence time is relatively small, which does not allow reaching a high percentage of fuel consumption. This explains why not all the fuel was consumed during this fast fire propagating uphill.

On the other hand, even though the fire occurred under unfavorable propagation conditions, with relatively high fuel moisture and relative humidity (FMC = 65% and RH = 82%) and low ambient air temperature (6 °C), the fire was characterized by a fire intensity larger than 6 MW/m (according to any evaluation method). This threshold value corresponds to the transition between "high" and "very high" fire danger index [28]. Indeed, in a fire fighting context, this value (6 MW/m) corresponds more or less to the efficiency limit of aerial means for the direct attack of a head fire (ranging between 3 and 10 MW/m depending on the spotting activity) [52]. Consequently, even if the wind speed was quite moderate (U_{10} = 1.98 m/s), and the conditions were unfavorable for fire propagation, this experiment confirms the fact that such fire can exhibit a dangerous behavior even in winter because it occurs along a steep slope (28°).

7. Conclusions

This paper presents a high-intensity experimental fire carried out during a field-scale experiment on a 28° sloped terrain, in the context of the winter prescribed burns campaign managed by the local firefighter service in the north-western region of Corsica. The paper describes thoroughly the used methodology as well as the collected measurements. The relevance of the numerical simulation in the case of high-intensity wildfire was demonstrated by numerically reproducing this experiment, using a completely physical 2D wildfire model (FireStar2D). The ROS was evaluated both experimentally and numerically, as well as the radiative and convective heat fluxes received by three distant targets, placed at the end of the plot. Numerical predictions were in fairly good agreement with experimental results. Moreover, the numerical prediction of heat transfer received by the unburned vegetation showed that the convection was the main mechanism of vegetation preheating. The fire intensity, evaluated experimentally and calculated numerically, was higher than 7 MW/m, which places this experimental fire in the "very high" despite the unfavorable conditions of fire propagation. The analysis of the dimensional Byram's convection number N_C, based on the fire line intensity, indicates that the fire regime was wind driven despite the low wind speed, and this is due to the steep slope and the resulting flame attachment to the fuel bed.

Only the global characteristics of this experimental fire were reported in this paper; other aspects, such as the shape of the fire front and temperature measurements, will be addressed in a future paper and compared to the predictions obtained from 2D and 3D numerical simulations. Also, further experimental studies are planned in the near future in order to better understand the behavior of high intensity wildfires.

Funding

This work was funded by the Corsican Region and the French state in the framework of the collaborative project GOLIAT (CPER: 40031).

Author contributions

Conceptualization, all the authors; **methodology**, Jean-Louis Rossi, Gilbert Accary, Lucile Rossi, Jacky Fayad, Nicolas Frangieh; **software**, Jacky Fayad, Carmen Awad, Nicolas Frangieh, Gilbert Accary, Lucile Rossi; **validation**, all the authors; **formal analysis**, all the authors; **writing—original draft preparation**, Jean-Louis Rossi, Jacky Fayad, Nicolas Frangieh, Carmen Awad, François-Joseph Chatelon, Gilbert Accary; **writing—review and editing**, Jean-Louis Rossi, Jacky Fayad, Nicolas Frangieh, Carmen Awad, François-Joseph Chatelon, Gilbert Accary; **supervision**, Jean-Louis Rossi, Gilbert Accary, Dominique Morvan. All authors have read and agreed to the published version of the manuscript."

Declaration of competing interest

The authors declare that they have no known competing financial interests or personal relationships that could have appeared to influence the work reported in this paper.

Acknowledgements

This field experiment required the cooperation of many people and would not have been possible without the assistance of the Forestry Service Department of North-Corsica (SIS2B) staff who selected the site, constructed firebreaks, protected the area, conducted the burning, and carried out fire suppression when spotting occurred with the collaboration of the Corsican DFCI (Défense de la Forêt Contre l'Incendie) Group. The authors would particularly to thank firefighter Patric Botey who supported this project since its beginning.

References

[1] F. di Castri, Mediterranean-type Shrublands of the World, Elsevier, Amsterdam, 1981.
[2] R.P. Benson, J.O. Roads, D.R. Weise, Chapter 2 climatic and weather factors affecting fire occurrence and behavior, in: A. Bytnerowicz, M.J. Arbaugh, A. R. Riebau, C. Andersen (Eds.), Dev. Environ. Sci., Elsevier, 2008, pp. 37–59, https://doi.org/10.1016/S1474-8177(08)00002-8.
[3] W.T. Sommers, S.G. Coloff, S.G. Conard, Synthesis of Knowledge: Fire History and Climate Change, 2011. http://www.firescience.gov/JFSP_fire_history.cfm.
[4] A. Mariotti, Y. Pan, N. Zeng, A. Alessandri, Long-term climate change in the Mediterranean region in the midst of decadal variability, Clim. Dynam. 44 (2015) 1437–1456, https://doi.org/10.1007/s00382-015-2487-3.
[5] S. Russo, J. Sillmann, E.M. Fischer, Top ten European heatwaves since 1950 and their occurrence in the coming decades, Environ. Res. Lett. 10 (2015), https://doi.org/10.1088/1748-9326/10/12/124003.
[6] F. Giorgi, Climate change hot-spots, Geophys. Res. Lett. 33 (2006) 1–4, https://doi.org/10.1029/2006GL025734.
[7] A. Ganteaume, R. Barbero, M. Jappiot, E. Maillé, Understanding future changes to fires in southern Europe and their impacts on the wildland-urban interface, J. Saf. Sci. Resil. 2 (2021) 20–29, https://doi.org/10.1016/j.jnlssr.2021.01.001.
[8] A. Ganteaume, M. Jappiot, What causes large fires in Southern France, For. Ecol. Manage. 294 (2013) 76–85, https://doi.org/10.1016/j.foreco.2012.06.055.
[9] W.M. Jolly, M.A. Cochrane, P.H. Freeborn, Z.A. Holden, T.J. Brown, G. J. Williamson, D.M.J.S. Bowman, Climate-induced variations in global wildfire danger from 1979 to 2013, Nat. Commun. 6 (2015) 11, https://doi.org/10.1038/ncomms8537.
[10] F.M.C. Castro Rego, J.M. Moreno Rodriguez, V.R. Vallejo Calzada, G. Xanthopoulos, Forest Fires - Sparking Firesmart Policies in the EU, Research &, Publications Office of the European Union, Luxembourg, 2018, https://doi.org/10.2777/181450.
[11] G.J. Cary, R.E. Keane, R.H. Gardner, S. Lavorel, M.D. Flannigan, I.D. Davies, C. Li, J.M. Lenihan, T.S. Rupp, F. Mouillot, Comparison of the sensitivity of landscape-fire-succession models to variation in terrain, fuel pattern, climate and weather, Landsc. Ecol. 21 (2006) 121–137, https://doi.org/10.1007/s10980-005-7302-9.
[12] European Science & Technology Advisory Group, Evolving Risk of Wildfires in Europe - the Changing Nature of Wildfire Risk Calls for a Shift in Policy Focus from Suppression to Prevention, 2020. Brussels, Belgium, https://www.undrr.org/publication/evolving-risk-wildfires-europe-thematic-paper-european-science-technology-advisory.
[13] G. Xanthopoulos, M. Athanasiou, A tale of two fires and a seaside tragedy, Wildfire Mag 28 (2019) 18–21.
[14] J.-H. Balbi, F.J. Chatelon, J.L. Rossi, A. Simeoni, D.X. Viegas, C. Rossa, Modelling of eruptive fire occurrence and behaviour, J. Environ. Sci. Eng. B Former. Part J. Environ. Sci. Eng. 3 (2014) 115–132.
[15] M.E. Alexander, Calculating and interpreting forest fire intensities, Can. J. Bot. 60 (1982) 349–357, https://doi.org/10.1139/b82-048.
[16] F. Tedim, V. Leone, M. Amraoui, C. Bouillon, M. Coughlan, G. Delogu, P. Fernandes, C. Ferreira, S. McCaffrey, T. McGee, J. Parente, D. Paton, M. Pereira, L. Ribeiro, D. Viegas, G. Xanthopoulos, Defining extreme wildfire events: difficulties, challenges, and impacts, Fire 1 (2018) 9, https://doi.org/10.3390/fire1010009.
[17] UNDRR, Sendai Framework for Disaster Risk Reduction 2015-2030, 2015. Geneva, Switzerland.
[18] M.A. Finney, J. Forthofer, I.C. Grenfell, B.A. Adam, N.K. Akafuah, K. Saito, A study of flame spread in engineered cardboard fuelbeds: Part I: correlations and observations, in: Seventh International Symposium on Scale Modeling (ISSM-7); Hirosaki, Japan; 6-9 August, 2013, International Scale Modeling Committee, 2013, p. 10.
[19] N. Frangieh, G. Accary, D. Morvan, S. Méradji, O. Bessonov, Wildfires front dynamics: 3D structures and intensity at small and large scales, Combust. Flame 211 (2020) 54–67cl, https://doi.org/10.1016/j.combustflame.2019.09.017.
[20] N. Liu, J. Wu, H. Chen, X. Xie, L. Zhang, B. Yao, J. Zhu, Y. Shan, Effect of slope on spread of a linear flame front over a pine needle fuel bed: experiments and modelling, Int. J. Wildland Fire 23 (2014) 1087–1096, https://doi.org/10.1071/WF12189.
[21] C. Awad, D. Morvan, J.-L. Rossi, T. Marcelli, F.J. Chatelon, F. Morandini, J.-H. Balbi, Fuel moisture content threshold leading to fire extinction under marginal conditions, Fire Saf. J. 118 (2020) 11, https://doi.org/10.1016/j.firesaf.2020.103226.
[22] C. Awad, N. Frangieh, T. Marcelli, G. Accary, D. Morvan, S. Meradji, F.-J. Chatelon, J.-L. Rossi, Numerical study of the moisture content threshold under prescribed burning conditions, Fire Saf. J. 122 (2021), https://doi.org/10.1016/j.firesaf.2021.103324. In Press.
[23] Jorger Raposoa, Domingos X. Viegasa, Xiaodong Xieb, Almeidaa Miguel, Naian Liu, Analysis of the jump fire produced by the interaction of two oblique fire fronts: comparison between laboratory and field cases, Adv. For. Fire Res. (2014) 1743–1748, uri, http://hdl.handle.net/10316.2/34140.
[24] Advances in forest fire research 2018, in: D.X. Viegas (Ed.), Adv. for. Fire Res., vol. 2018, 2018, https://doi.org/10.14195/978-989-26-16-506.
[25] J.B. Marsden-Smedley, W.R. Catchpole, Fire behaviour modelling in tasmanian buttongrass moorlands ii. Fire behaviour, Int. J. Wildland Fire 5 (1995) 215–228, https://doi.org/10.1071/WF9950215.
[26] X. Silvani, F. Morandini, Fire spread experiments in the field: temperature and heat fluxes measurements, Fire Saf. J. 44 (2009) 279–285, https://doi.org/10.1016/J.FIRESAF.2008.06.004.
[27] B. Butler, C. Teske, D. Jimenez, J. O'Brien, P. Sopko, C. Wold, M. Vosburgh, B. Hornsby, E. Loudermilk, Observations of energy transport and rate of spreads from low-intensity fires in longleaf pine habitat - RxCADRE 2012, Int. J. Wildland Fire 25 (2016) 76–89, https://doi.org/10.1071/WF14154.
[28] D. Morvan, S. Méradji, G. Accary, Physical modelling of fire spread in Grasslands, Fire Saf. J. 44 (2009) 50–61, https://doi.org/10.1016/j.firesaf.2008.03.004.
[29] V. Leroy-Cancellieri, P. Augustin, J.B. Filippi, C. Mari, M. Fourmentin, F. Bosseur, F. Morandini, H. Delbarre, Evaluation of wildland fire smoke plume dynamics and aerosol load using UV scanning lidar and fire-atmosphere modelling during the Mediterranean Letia 2010 experiment, Nat. Hazards Earth Syst. Sci. 14 (2014) 509–523, https://doi.org/10.5194/nhess-14-509-2014.
[30] M. Cohen, E. Rigolot, J.C. Valette, From the vegetation to the inputs of a fire model: fuel modelling for wildland-urban interface management, Warm Int. Work. "Forest Fires Wildland-Urban Interface Rural Areas Eur. an Integr. Plan. Manag. Challenge." (2004) 113–120.
[31] D. Morvan, Numerical study of the effect of fuel moisture content (FMC) upon the propagation of a surface fire on a flat terrain, Fire Saf. J. 58 (2013) 121–131, https://doi.org/10.1016/j.firesaf.2013.01.010.
[32] A.M. Grishin, Mathematical Modeling of Forest Fires and New Methods of Fighting Them, Publishing House of the Tomsk University, Tomsk, Russia, 1996. https://books.google.fr/books?id=MtScGwAACAAJ.
[33] H.P. Hanson, M.M. Bradley, J. Bossert, R.R. Linn, L.W. Younker, The potential and promise of physics-based wildfire simulation, Environ. Sci. Pol. 3 (2000) 161–172.
[34] D. Morvan, J.L. Dupuy, Modeling the propagation of a wildfire through a Mediterranean shrub using a multiphase formulation, Combust. Flame 138 (2004) 199–210, https://doi.org/10.1016/j.combustflame.2004.05.001.
[35] D. Morvan, S. Meradji, G. Accary, Wildfire behavior study in a mediterranean pine stand using a physically based model, Combust. Sci. Technol. 180 (2008) 230–248, https://doi.org/10.1080/00102200701600978.
[36] D. Morvan, J.L. Dupuy, Modeling of fire spread through a forest fuel bed using a multiphase formulation, Combust. Flame 127 (2001) 1981–1994, https://doi.org/10.1016/S0010-2180(01)00302-9.
[37] D. Morvan, Physical phenomena and length scales governing the behaviour of wildfires: a case for physical modelling, Fire Technol. 47 (2011) 437–460, https://doi.org/10.1007/s10694-010-0160-2.
[38] N. Frangieh, D. Morvan, S. Meradji, G. Accary, O. Bessonov, Numerical simulation of grassland fires behavior using an implicit physical multiphase model, Fire Saf. J. 102 (2018) 37–47, https://doi.org/10.1016/j.firesaf.2018.06.004.
[39] D. Morvan, G. Accary, S. Meradji, N. Frangieh, O. Bessonov, A 3D physical model to study the behavior of vegetation fires at laboratory scale, Fire Saf. J. 101 (2018) 39–52, https://doi.org/10.1016/j.firesaf.2018.08.011.
[40] M.S. Owen, ASHRAE Handbook: Fundamentals, American Society of Heating, Refrigeration and Air-Conditioning Engineers, 2009, 2009.
[41] G.M. Byram, in: K.P. Davis (Ed.), Forest Fire Control and Use, McGraw-Hill, New York, 1959.

[42] M.E. Alexander, M.G. Cruz, Fireline Intensity, Encycl. Wildfires Wildland-Urban Interface Fires, 2020, pp. 453–460, https://doi.org/10.1007/978-3-319-52090-2_52.
[43] R.M. Nelson, Re-analysis of wind and slope effects on flame characteristics of Mediterranean shrub fires, Int. J. Wildland Fire 24 (2015) 1001–1007.
[44] D. Morvan, N. Frangieh, Wildland fires behaviour: wind effect versus Byram's convective number and consequences upon the regime of propagation, Int. J. Wildland Fire 27 (2018) 636–641, https://doi.org/10.1071/WF18014.
[45] R.M. Nelson, An effective wind speed for models of fire spread, Int. J. Wildland Fire 11 (2002) 153–161, https://doi.org/10.1071/WF02031.
[46] D.X. Viegas, Advances in forest fire research, in: Advances in Forest Fire Research, 2014, https://doi.org/10.14195/978-989-26-0884-6.
[47] M.G. Cruz, M.E. Alexander, Uncertainty associated with model predictions of surface and crown fire rates of spread, Environ. Model. Software 47 (2013) 16–28, https://doi.org/10.1016/j.envsoft.2013.04.004.
[48] P.N. Cheney, Fire behaviour, in: A. Gill, R. Grooves, I. Noble (Eds.), Fire Aust. Biota, Australian Academy of Science, 1981, pp. 151–175. Canberra, ACT.
[49] K. Chatto, K.G. Tolhurst, A Review of the Relationship between Fireline Intensity and the Ecological and Economic Effects of Fire, 2004. Melbourne.
[50] J.K. Burrows, Experimental Development of a Fire Management Model for Jarrah (Eucalyptus Marginata Ex Sm) Forest, Australian National University, Canberra, 1994.
[51] A. Dahale, S. Ferguson, B. Shotorban, S. Mahalingam, Effects of distribution of bulk density and moisture content on shrub fires, Int. J. Wildland Fire 22 (2013) 625–641, https://doi.org/10.1071/wf12040.
[52] K. Hirsch, D. Martell, A review of initial attack fire crew productivity and effectiveness, Int. J. Wildland Fire 6 (1996) 199–215, https://doi.org/10.1071/WF9960199.